

# The HI environment of the Sculptor dwarf spheroidal galaxy

Antoine Bouchard

*Département de physique and Observatoire du mont Mégantic, Université de Montréal, C.P. 6128, Succ. Centre-ville, Montréal, Québec, Canada H3C 3J7, and Australia Telescope National Facility, PO Box 76, Epping, NSW 1710, Australia*

bouchard@astro.umontreal.ca

Claude Carignan

*Département de physique and Observatoire du mont Mégantic, Université de Montréal, C.P. 6128, Succ. Centre-ville, Montréal, Québec, Canada H3C 3J7*

carignan@astro.umontreal.ca

Sergey Mashchenko

*Département de physique and Observatoire du mont Mégantic, Université de Montréal, C.P. 6128, Succ. Centre-ville, Montréal, Québec, Canada H3C 3J7*

syam@astro.umontreal.ca

## ABSTRACT

New observations of the neutral hydrogen (HI) in and around the line of sight of the Sculptor dwarf spheroidal (dSph) are presented. The data obtained with the single-dish Parkes telescope cover a large area of  $7^\circ \times 7^\circ$  in the direction of the dwarf, and have resolutions of  $15.5' \times 1.12 \text{ km s}^{-1}$ . The Australia Telescope Compact Array was used to map a smaller area of  $2.2^\circ \times 2.2^\circ$  centered on the direction of the dwarf with higher resolutions ( $350'' \times 140'' \times 1.65 \text{ km s}^{-1}$ ). Many HI structures having velocities outside the range of the normal Galactic disk velocities were detected, including the two Sculptor clouds (northeast and southwest) of Carignan et al. (1998, C98). The present study shows the total extent of the C98 clouds. We derived heliocentric radial velocities for the NE and SW clouds of  $100.2 \pm 0.9 \text{ km s}^{-1}$  and  $105.1 \pm 0.3 \text{ km s}^{-1}$ , respectively. The intensity-weighted mean HI velocity for both clouds is  $104.1 \pm 0.4 \text{ km s}^{-1}$ .

Three different hypotheses concerning the association of the C98 Sculptor clouds were considered. The case for the clouds belonging to the Sculptor group of galaxies is found to be inconsistent with the observational data. The probability of the C98 Sculptor clouds to be Milky Way features at anomalous velocities (HVCs) superimposed by chance on the Sculptor dSph is estimated to be less than 2%. The third hypothesis assumes that the clouds are physically associated with the Sculptor dSph, and is supported by the following evidences: (a) the radial velocities for both clouds are very

close to the optical velocity of the Sculptor dSph ( $\Delta V = 4 \pm 3 \text{ km s}^{-1}$ ). (b) 88% of the total HI flux is contained within the optical radius of the galaxy, and (c) the clouds are located symmetrically relative to the center of the Sculptor dSph. Arguments are presented that the C98 Sculptor clouds are still gravitationally bound to the dwarf galaxy, and are part of its interstellar medium. The mass of each cloud is  $(4.1 \pm 0.2) \times 10^4 \text{ M}_\odot$  (NE cloud) and  $(1.93 \pm 0.02) \times 10^5 \text{ M}_\odot$  (SW cloud) at the Sculptor dSph distance (79 kpc).

*Subject headings:* galaxies: dwarf — galaxies: individual (Sculptor) — ISM: HI — Local Group — techniques: interferometric

## 1. Introduction

Dwarf galaxies are the most numerous type of galaxies in the Universe. Recently, the interest for the lowest luminosity dwarfs has been renewed, both on the observational and on the theoretical sides, in part because these stellar systems have the spatial scale at which the predictions of the presently favored  $\Lambda$ CDM cosmology have the largest discrepancies with observations. Most notably,  $\Lambda$ CDM simulations overpredict the number of low mass galaxies in the Milky Way and M31 halos (Moore et al. 1999). Another difficulty is the cuspy density profile of simulated halos, which is at odds with the almost flat cores observed in the inner few kiloparsecs of disk galaxies (de Blok et al. 2001; Blais-Ouellette et al. 2001).

Low luminosity dwarfs in the Local Group are classified as dwarf irregulars (dIrr), dwarf spheroidals (dSph), or intermediate type dwarfs (dIrr/dSph) (Mateo 1998). dIrr galaxies are gas rich and the HI is often seen in rings surrounding the optical center (Carignan 1998; Young & Lo 1997) or bubble like structures (LeoA, Young & Lo 1996) and their complex Star Formation History (SFH) can easily be explained. For dSph galaxies, the data are harder to explain. The ISM is required to support the complex SFH (Grebel 1998) of these objects and until now, very few of them are actually known to contain HI. This is what led Blitz & Robishaw (2000) to believe “that all of the LG dwarf galaxies have had loosely bound HI envelopes” thus implicitly making a link between High Velocity Clouds, dSph, and dIrr.

In the Local Group, all dwarf galaxies less luminous than  $M_V \simeq -15^m$  and located within 250 kpc from a giant spiral (Milky Way or M31) are dSphs. All dIrr galaxies in the same luminosity range are isolated systems. This segregation of the dwarfs into dSphs and dIrrs according to their distance from giant spirals suggests that some (or many) environmental factors are at work. The most popular mechanisms discussed in the literature are total removal of the ISM by either tidal or ram pressure stripping (e.g. Blitz & Robishaw 2000). However, the total ISM removal cannot explain the puzzling situation with many dSphs, which have formed stars in the last 1-2 Gyrs, but have no HI gas around them which could have fueled the star formation.

Mashchenko, Carignan, & Bouchard (2003, hereafter MCB) proposed a possible solution for this puzzle. They showed that far ultraviolet (FUV) flux from spirals like the Milky Way and M31 can be strong enough to keep the ISM of satellite dSphs in a fully photoionized state for prolonged periods of time, and by assuming that many dSphs are massive enough (with the virial temperature  $T_{\text{vir}} \gtrsim 10^4$  K) to keep the photoionized gas gravitationally bound. Only during relatively short intervals of time, when the dSph moving along its orbit around the host galaxy is crossing the shadow produced by the HI disk of the host, can the ISM recombine and potentially form stars.

Any evidence for a physical association of HI gas with a low luminosity dSph galaxy would be crucial for understanding the factors governing the evolution of these systems. One of the most promising objects in this regard is the Sculptor dSph. Carignan et al. (1998, hereafter C98) detected two HI clouds in the vicinity of the dwarf, with radial velocities very similar to the optical velocity of the Sculptor dSph. Their observations of a  $\sim 0^{\circ}5$  field covered only a small portion of the stellar body of the dwarf which has a major axis of  $\sim 2^{\circ}5$  (Irwin & Hatzidimitriou 1995). This prevented the authors from giving a conclusive evidence for a physical association of the gas with the Sculptor dSph. New HI observations with a much larger spatial coverage were required to see the full extent of the clouds, and to make sure that these clouds were not Galactic HVCs.

Here we present new observations made with the Australia Telescope Compact Array (ATCA) and the Parkes single-dish telescope covering large areas around the Sculptor dwarf –  $7^{\circ} \times 7^{\circ}$  for Parkes and  $2^{\circ} \times 2^{\circ}$  for the ATCA. We analyze all HI structures detected in this area, and argue that the new data strengthen the case for the physical association of the two C98 clouds with the dSph while the others are most likely unrelated to the Sculptor dSph. By combining our new HI data with the data of Weiner, Vogel, & Williams (2001) on  $\text{H}_{\alpha}$  emission from the Sculptor clouds, we also give evidence in support of the radiation harassment scenario of MCB.

## 2. Observations of HI in the direction of the Sculptor dSph

### 2.1. Previous observations

C98 made two sets of observations. First, they used the Parkes single dish radio-telescope and pointed it directly at the center of the galaxy. They used the source PKS1934-638 as a flux calibrator and they had a velocity resolution of  $1.65 \text{ km s}^{-1}$ . Their 100 minutes integration on source resulted in a detection limit of  $100 \text{ M}_{\odot}$ . The spectrum they obtained revealed  $\sim 10^4 \text{ M}_{\odot}$  of HI, at a velocity of  $V_{\odot} = 112 \text{ km s}^{-1}$ . But the  $\sim 15'$  beam did not cover all the optical extent of the Sculptor dSph (which has a tidal radius of  $\sim 1^{\circ}3$ , see Table 1) and it was not large enough to get a complete sampling of what is believed to be the gas associated with the dwarf.

Their second set of observations was obtained with the ATCA using the array configuration 210 which resulted in a spatial resolution of  $240''$  and a velocity resolution of  $1.65 \text{ km s}^{-1}$ . This

Table 1: The Sculptor dSph physical parameters.

Parameter	Value
RA (J2000)	1 <sup>h</sup> 00 <sup>m</sup> 09 <sup>s</sup> .4
DEC (J2000)	−33°42'33"
Galactic longitude, l	287.53
Galactic latitude, b	−83.16
Heliocentric distance <sup>a</sup>	79 ± 4 kpc
Isophotal major axis <sup>b</sup> , $D_{25}$	40'
Core radius <sup>c</sup> , $r_c$	5.8 ± 1.6
Tidal radius <sup>c</sup> , $r_t$	76.5 ± 5.0
Major-axis position angle <sup>c</sup>	99° ± 1°
Optical radial velocity <sup>a</sup> , $V_{\odot}^{opt}$	108 ± 3 km s <sup>−1</sup>
Proper motion velocity <sup>d</sup> , $V_{prop}$	210 ± 125 km s <sup>−1</sup>
Proper motion position angle <sup>d</sup>	40° ± 24°

<sup>a</sup>Mateo 1998

<sup>b</sup>de Vaucouleurs et al. 1991

<sup>c</sup>Irwin & Hatzidimitriou 1995

<sup>d</sup>Schweitzer et al. 1995

yielded an HI mass of  $3.0 \times 10^4 M_{\odot}$ , at a velocity of  $102 \pm 5 \text{ km s}^{-1}$ . But inevitable short spacing effects appeared in the data which made the authors believe that they missed a non-negligible fraction of the HI. Moreover a large fraction of the detected HI lied close to the half-power beam width (FWHM=  $33'$ ).

## 2.2. New Parkes data

The 64 m Parkes radio-telescope was used, equipped with a 21 cm multibeam receiver in a narrowband mode. The total bandwidth of 8 MHz was divided in 2048 channels, resulting in a velocity increment of  $0.82 \text{ km s}^{-1}$  between each channel of the cube for a total velocity coverage of  $1600 \text{ km s}^{-1}$  centered on  $V_{\odot} = -200 \text{ km s}^{-1}$ . A region of  $7^\circ \times 7^\circ$  was mapped around the Sculptor dSph at a beam resolution of  $15.5'$  and a velocity resolution of  $1.12 \text{ km s}^{-1}$ , using frequency switching observations.

The reduction pipeline provided with the AIPS++ package was used to calibrate the data (task "Livedata") and to grid and form the cube (task "Gridzilla"). Both tasks are part of the standard HIPASS data acquisition system (Barnes et al. 2001). For the bandpass calibration, the data were Hanning smoothed and the median value of the baseline was subtracted.

## 2.3. New ATCA data

The ATCA is located in Narrabri, Australia. It consists of six 22 meters antennae on an East-West track. This aperture synthesis array was used in the 0.210 configuration, with baselines ranging from 31 to 214 meters, giving the maximum possible weight to large structures.

The data cube is a 64 pointing mosaic centered on a frequency of 1420 MHz. The array configuration, along with a total bandpass of 8 MHz divided in 1024 channels resulted in physical resolutions of  $350'' \times 140'' \times 1.65 \text{ km s}^{-1}$ . The source PKS1934-638 was used as a flux calibrator while PKS0008-421 was the phase calibrator. The Miriad package was used to edit and calibrate the data.

## 2.4. Data Analysis

Figure 1 shows a wide field image taken with the Parkes radiotelescope equipped with the narrowband multibeam receiver. The region in the direction of the Sculptor dSph is heavily populated with HI features. Aside from the Sculptor (NE and SW) clouds, only one HI structure from Figure 1 has been previously associated with an optical object — the spiral galaxy NGC 300 from the Sculptor group. Many other features are catalogued as HVCs by Putman et al. (2002). The radial velocities for each feature marked in Figure 1 are listed in Table 2.

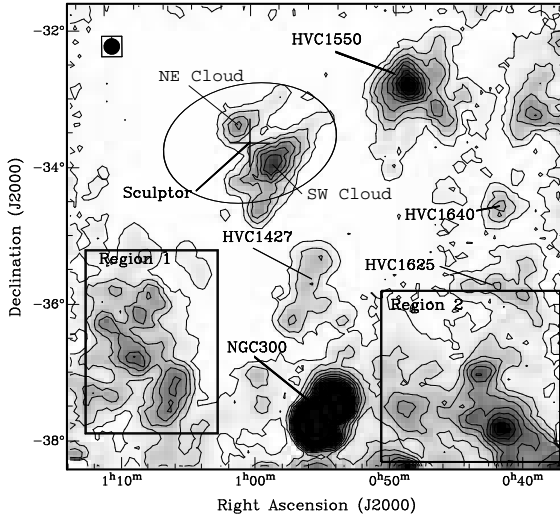


Fig. 1.— Parkes narrowband integrated HI map. The contour levels are  $(1, 5, 10, 15, \dots, 40) \times 10^{18} \text{ cm}^{-2}$ . We show the locations of some HVCs from the catalog of Putman et al. (2002), and define two regions of comparable velocities — Region 1 and Region 2. The ellipse shows the optical extent of the Sculptor dSph (Irwin & Hatzidimitriou 1995). The cross marks the location of the optical center of Sculptor.

This study will concentrate on the two HI features closest to the optical center of the Sculptor dSph — the NE and SW clouds (see Figure 1). A close-up view of the Sculptor clouds is shown in Figure 2. This is a higher spatial resolution image taken with the ATCA interferometer. The integrated spectra for the clouds are shown in Figure 3. The velocity information extracted from the spectra is summarized in Table 5. The table also contains HI mass estimates, based on the assumption that the clouds are located at the distance of the Sculptor dSph (79 kpc, see Table 1).

Parts of the Sculptor clouds were observed by C98. In our present study, we can see the full extent of the clouds. They have larger sizes and masses (Table 5) than those reported by C98, but appear to be almost completely contained within the optical extent of the Sculptor dSph (88% of the total flux). The existence of the third (central) cloud of C98 with low detection significance is not confirmed with our new data, which is evident from the spectrum of the central  $15' \times 15'$  area shown in Figure 3d and the corresponding parameters given in Table 5. This central region has a slightly negative integral flux (resulted in a negative mass in Table 5). This is caused by an imperfect continuum subtraction performed on the image. The signal does not significantly come out of the noise (Figure 3d).

The lack of short spacings in the ATCA data is most obvious in panels b) and c) of Figure 3. The 210 configuration of the array used for the observations is not sensitive to scales larger than

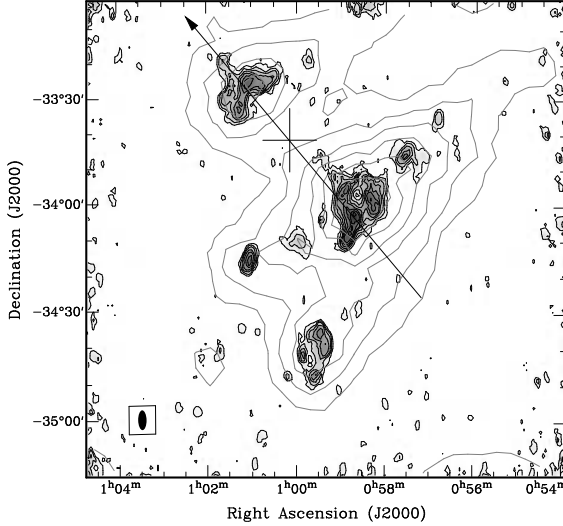


Fig. 2.— ATCA integrated HI (grey-scale image and black contours) overlayed with the Parkes data from Figure 1 (grey contours). The contours for the ATCA data have levels  $(5, 10, 15, \dots, 40) \times 10^{18} \text{ cm}^{-2}$ . The arrow shows the direction of the proper motion of the Sculptor dSph from Schweitzer et al. (1995).

$\sim 30'$ , resulting in the mass of the SW cloud being significantly underestimated (Table 5). The NE cloud with a size  $\sim 22'$  has less suffered from this effect.

Figure 4 shows a slice along the velocity axis through both the ATCA and the Parkes data sets. The slice passes through the center of the Sculptor dSph along the proper motion direction (arrow in Figure 2). We clearly see the NE cloud (on the left side) and the SW cloud (on the right side). The cross marks the position of the galactic center and the velocity of the dwarf. It is clear from this figure that both clouds are distributed symmetrically relative to the dwarf's center and have similar velocities, though the velocity of the NE cloud tends to be slightly less than that of the SW cloud.

Velocity information can also be found in Figure 5. This velocity map from the Parkes data shows the two main Sculptor clouds and a third one (HVC 1550) close to the dwarf. Figure 6 shows the dispersion of the HI gas of the Sculptor dSph surroundings. The maximum dispersion values of every feature identified in Figure 1 are listed in Table 2.

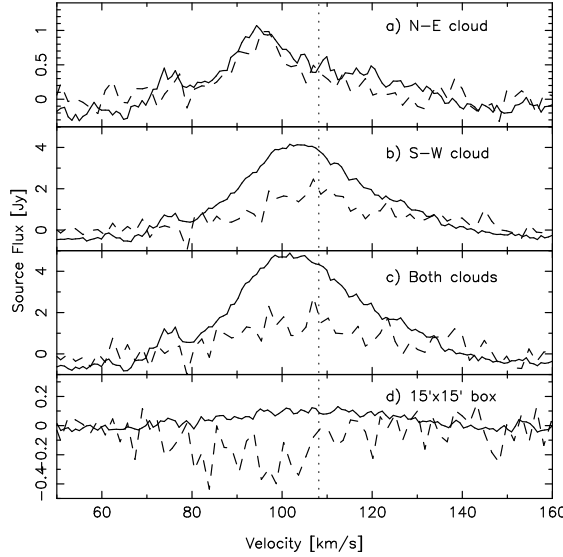


Fig. 3.— Four spectra, taken both from the Parkes (solid line) and ATCA (dashed line) data sets. Panels a) and b) show the spectra integrated over the North-East and South-West clouds, respectively, panel c) shows the total spectrum, and panel d) shows the spectrum for a  $15'$  by  $15'$  box centered on the dwarf. The vertical dotted line corresponds to the optical radial velocity of the Sculptor dSph.

### 3. Discussion

#### 3.1. Physical association of the Sculptor clouds

The quality of our present data on the HI distribution in the line of sight of the Sculptor dSph gives us an opportunity to address the issue of the physical association of HI gas with a dSph in a more conclusive manner than any previous study. In the past, the attempts to associate nearby HI gas with dSph galaxies have been hampered by some of the following factors: lack of spatial coverage (C98), low angular and velocity resolutions (Blitz & Robishaw 2000), and lack of stellar radial velocity information (Oosterloo, Da Costa, & Staveley-Smith 1996). In this study, we achieve both sufficiently large spatial coverage ( $7^\circ \times 7^\circ$ , with the area covered being 14 times larger than the area of the Sculptor stellar body) and high angular and velocity resolutions ( $5'.8 \times 2'.3 \times 1.65 \text{ km s}^{-1}$ ) by combining the single-dish Parkes with interferometric ATCA observations. In addition, the stellar radial velocity of the Sculptor dSph is now known to a high accuracy (Table 1).

The locations and radial velocities of the NE and SW clouds leave us with only two possible alternatives in regards to the physical association with the Sculptor dSph: the case of a larger distance (the clouds belong to the Sculptor group of galaxies), and the case of a smaller distance (the clouds are Galactic HVCs). We will consider both possibilities in turn.

Table 2: Properties of the HI features of Figure 1.

	$V_\odot$ (km s $^{-1}$ )	$\sigma_{max}$ (km s $^{-1}$ )
NE cloud (HVC 1321)	100	6.0
SW cloud (HVC 1353)	105	9.9
NGC 300	145	37.6
HVC 1427	135	7.9
HVC 1550	117	11.0
HVC 1625	169	21.5
HVC 1640	175	13.4
Region 1 (broad region)	121	9.0
Region 1 (artifact)	121	21.0
Region 2	40	4.4

At the distances of the Sculptor group members (1.7 – 4.4 Mpc, Jerjen et al. 1998) the clouds would have very large size ( $\sim 25$  – 60 kpc) and total mass ( $[1$  – 5]  $\times 10^8$  M $_\odot$ ). Isolated intergalactic HI clouds of this size are not known. Moreover, the H $\alpha$  flux of 0.22 R, detected in the densest part of the SW cloud (see Section 3.2), is too large to be caused by the metagalactic ionizing radiation background, and is most naturally explained by the impact of the LyC radiation from the Milky Way, implying a small distance to the clouds of  $\lesssim 100$  kpc. The clouds also cannot belong to a galaxy located at the distance of the Sculptor group: a gas-rich galaxy of this size would be a disk galaxy, which is at odds with both the irregular shape of the clouds and the absence of a clear rotation signature. We conclude that the Sculptor group hypothesis appears to be inconsistent with the available data.

The second alternative — the SW and NE clouds being HVCs — is more difficult to discard. HVCs are clouds that do not fit any simple galactic rotation models. These clouds are often associated in large HVC complexes that are believed to be of similar origin. One of these complexes, the Magellanic Stream, has many components near the Sculptor dSph, but its velocity in this direction,  $\sim -60$  km s $^{-1}$  (Mathewson & Ford 1984), makes it a very unlikely association.

One should also realize that the majority of the HVCs is not part of an HVC complex. What is seen in Figure 1 could be independent HVCs which happened to be in the line of sight of the Sculptor dSph and have radial velocities very close to the radial velocity of the dwarf. We estimated the probability of such an event in the following manner. As can be seen in Table 3, the number  $N$  of HVCs from the catalog of Putman et al. (2002) located within  $R_0 = 10^\circ$  from the Sculptor dSph and having heliocentric radial velocities within the interval  $V = +80 \dots +210$  km s $^{-1}$  is  $N = 26$  (excluding the Sculptor clouds). We considered the NE and SW clouds to be one cloud. The center of mass of this cloud is located at the distance  $R_1 = 0^\circ.318$  from the center of the Sculptor dSph, and

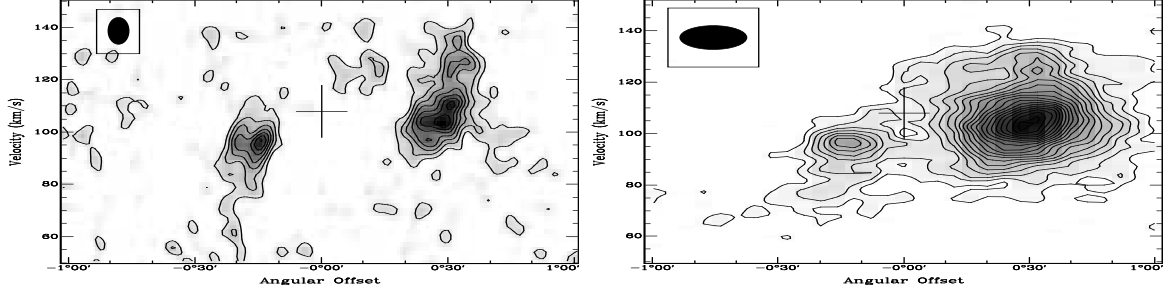


Fig. 4.— A cut through the ATCA (top panel) and Parkes narrowband (bottom panel) data sets. The slice is  $12'$  wide in both cubes and is aligned with the galaxy's proper motion (position angle of  $40^\circ$ , see Figure 2). The ATCA data have been smoothed in velocity to  $11.41 \text{ km s}^{-1}$  and have contour levels from 10 to 70 mJy by steps of 10 mJy. The narrowband data are smoothed in velocity to  $10.66 \text{ km s}^{-1}$  and the levels are from 2.5 to 50 mJy at every 2.5 mJy.

has a radial velocity of  $104 \text{ km s}^{-1}$ , resulting in the difference  $\Delta V_1 = 4 \text{ km s}^{-1}$  between the stellar and HI velocities. Assuming that locations and radial velocities of the  $N$  HVCs are uncorrelated and distributed uniformly within the circle with the radius  $R_0$  and the velocity interval  $\Delta V_0$ , the probability  $P$  to find *at least one* HVC located within  $R_1$  from the center of the Sculptor dSph and having radial velocity within  $\Delta V_1$  from the velocity of the dwarf galaxy is given by the following expression:

$$P = 1 - \left[ 1 - \left( \frac{R_1}{R_0} \right)^2 \frac{2 \Delta V_1}{\Delta V_0} \right]^{N+1}. \quad (1)$$

(The exponent is  $N + 1$  because we also include the Sculptor cloud; the velocity interval  $\Delta V_1$  is multiplied by 2 because the difference in velocities can be both positive and negative.) In our case,  $\Delta V_0 = 130 \text{ km s}^{-1}$ , and the probability that the Sculptor cloud is an HVC is  $P = 0.17\%$ . Even if no velocity information was available and we had included all the clouds in Table 4 in our calculation, the probability would still only be  $P \sim 0.44\%$ . If we considered the Sculptor clouds to be two independent HVCs, the corresponding probability would be a few orders of magnitude lower. Of course, either one or both of our assumptions (absence of correlation, and uniform distribution) might prove to be wrong, so the probability  $P \sim 0.2\%$  derived above should be treated with caution.

There is one fundamental flaw in the above probability derivations. To obtain equation (1), we implicitly assumed that our choice of a dSph galaxy (Sculptor) is an unbiased one. In reality, there are other Galactic dSphs, and the reason we are so interested in Sculptor is because it happened to have HI gas in its vicinity with similar radial velocity. The correct question to ask would be: “What is the probability that at least one of the dSphs has at least one HVC in its vicinity, which is located as close (or even closer) to the dwarf galaxy (both spatially, and in radial velocity) as the Sculptor dSph cloud is?” To answer this question one would need to calculate corresponding

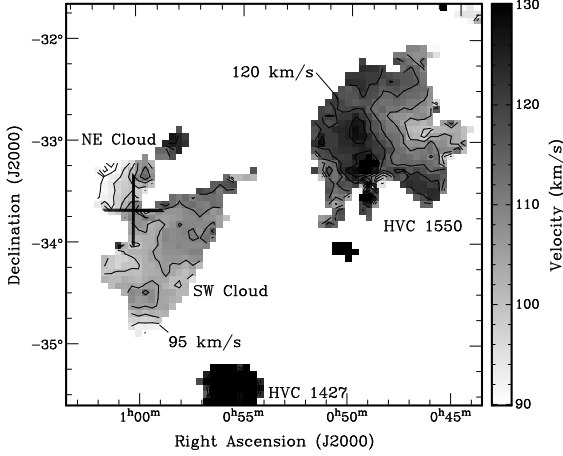


Fig. 5.— The velocity map for the Parkes narrowband data. The contours are separated by 5  $\text{km s}^{-1}$ , ranging from 90 to 130  $\text{km s}^{-1}$ . Only the closest clouds to the Sculptor dSph, in both velocity and position on the sky, have been included in this figure. The wide-field nature of this picture and the high discrepancy in the velocities of the clouds would make the full  $7^\circ \times 7^\circ$  Figure irrelevant to the discussion and velocity gradients undistinguishable.

individual probabilities  $P_i$  using equation (1) for the 8 known dSphs (we exclude Sagittarius as it appears to be in the process of being disrupted by the Galactic tidal field), and then to estimate the total probability as

$$P_{tot} = 1 - \prod_{i=1}^8 (1 - P_i). \quad (2)$$

Assuming for simplicity that the individual probabilities  $P_i$  are the same for all dSphs, and are equal to the derived above probability for the Sculptor dSph ( $P = 0.17\%$ ), the total probability is  $P_{tot} = 1 - (1 - P)^8 \simeq 1.4\%$ . Even in this more realistic approach, the probability of the Sculptor clouds being HVCs appears to be very low.

It is clear from Figure 6 and Table 2 that the Sculptor clouds are quite different from at least some of the other nearby features. NGC 300 is a spiral galaxy; its HI cannot be confused with other structures in Figure 6. The Milky Way's HI in that direction, although being near the South Galactic Pole line of sight, still has some leftover emission at  $+40 \text{ km s}^{-1}$ . This residual emission is relatively faint when compared with the bulk emission at  $0 \text{ km s}^{-1}$  but is still very bright when compared with other “background” sources. A careful inspection of the dataset reveals that Region 2 is such an extension and it is most likely some sort of feature from the Milky Way.

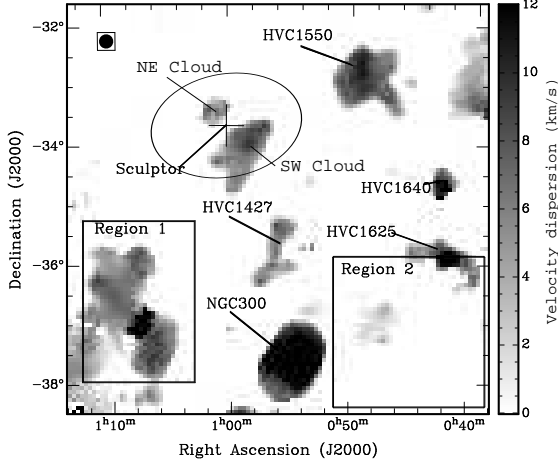


Fig. 6.— Velocity dispersions from the Parkes dataset.

HVC 1625 has two distinct components: a large ( $1^\circ$ ) filament with a low velocity dispersion and a compact (spatially unresolved) core with a higher dispersion. HVC 1640 is a compact object having a high dispersion, similar to HVC 1625. These objects have velocity structures that are very different from the other clouds seen in Figure 6. Therefore they are probably of different origin.

Region 1 is composed of two types of structure: a broad region with a low dispersion and a very high dispersion compact core. This apparently high dispersion value is artificially inflated by the overlap of two clouds with different velocities and should be treated as an artifact. The compact cloud is probably an extension of the Galactic HI, similar to the case of the Region 2. The other clouds of Region 1, HVC 1427 and HVC 1550 are all similar in size and kinematic structure to the Sculptor clouds. It is conceivable then that these clouds are part of a larger HI stream. The shape of the SW cloud also suggests that this link might be real. Analysis of the velocity field (Figure 5) suggests a velocity gradient between the SW cloud and HVC 1550. However, upon inspection of all HVCs (Table 3 and 4), there is no evidence for an HI stream in this region. The velocities of the nearby clouds are dispersed in an incoherent pattern.

One of the most interesting results obtained in the present work is the almost perfect agreement between the HI velocity for the both Sculptor clouds (Table 5) and the optical velocity of the dwarf (Table 1). The difference in velocities for the Parkes data is  $V_{\odot}^{opt} - V_{HI} = 4 \pm 3 \text{ km s}^{-1}$ . However, a kinematic agreement between HI clouds and dSph galaxies is to be regarded with caution. Alone, this should never be considered as an evidence for an HI association.

In the case of the Sculptor dSph, the fact that almost all of the detected HI emission is contained within the optical boundaries of the dwarf galaxy (Figure 1), the symmetric location of the two

clouds relative to the galactic center (Figure 2), the closeness of the radial velocities between the clouds and the dwarf, the low inferred probability  $P_{tot} \simeq 2\%$  for the clouds to be HVCs, and the presence of an arm coming out of the SW cloud and pointing in the direction of the Sculptor dSph center (Figure 2), strongly favor the physical association of the clouds and dwarf galaxy. However, in the absence of accurate distance measurements to the HI clouds, the HVC hypothesis remains a possible (though unlikely) alternative.

### 3.2. Nature of the Clouds associated with the Sculptor dSph

Having argued that the NE and SW clouds are physically associated with the Sculptor dSph, the important question to answer is whether the clouds are still gravitationally bound to the dwarf galaxy, or if they have been removed by some mechanism — either internal (winds from red giants, supernovae type Ia), or external (ram pressure stripping by the Galactic hot halo gas, Galactic tidal field).

The symmetric location of the clouds relative to the center of the Sculptor dSph along its proper motion vector (see Figure 2) appears to be consistent with the tidal removal picture. However, the orientation of the stellar body of the dwarf which has a comparable angular extent to that of the HI gas (see Figure 1) indicates that the tidal forces have not played a major part in shaping the galaxy. The biggest obstacle for another external removal mechanism — ram pressure stripping — is the presence of the NE cloud ahead of the proper motion (Figure 2).

An important observational evidence for the clouds being gravitationally bound to the dwarf would be a rotation signature for the gas. C98 speculated on the possibility of rotation of the NE and SW clouds around the center of the Sculptor dwarf. It is clear from Figure 4 that there is a velocity gradient between the two clouds. The classical Newtonian formula gives a central mass of  $\sim 6.7 \times 10^5 M_{\odot}$  when using the Parkes velocity information (rotation speed of  $2.5 \text{ km s}^{-1}$  at a distance of  $20'$ , see Table 5 and Figure 4). The ATCA velocity information gives an enclosed mass of  $2.7 \times 10^6 M_{\odot}$  with the same conditions but a rotation speed of  $5 \text{ km s}^{-1}$ . These estimates assume that the gas follow a circular orbit viewed edge on, therefore no projection effect on the distance or velocity of the clouds have been taken into account and the gas is considered to be neither infalling nor expanding. Mateo (1998) gives a total mass of  $6.4 \times 10^6 M_{\odot}$  for the Sculptor dSph. The inferred rotation speed values are comparable to or less than the internal velocity dispersion in the clouds (see Table 2). In this respect, the Sculptor dSph would be similar to low luminosity dIrr and dIrr/dSph galaxies, such as GR 8, Leo A, SagDIG, and LGS 3.

Our main argument against any HI removal scenario (either internal or external) is that the gas removal would not solve the ISM crisis in dSph galaxies (Mateo 1998). The alternative is that the NE and SW clouds are gravitationally bound to the Sculptor dSph, and are part of its ISM.

MCB proposed a scenario which can explain the statistical differences between the low luminosity dwarf galaxies in the Local Group. They showed that the FUV radiation escaping from

spiral galaxies can warm up and photoionize the ISM of their dSph satellites, quenching star formation and making the ISM virtually unobservable. Only during relatively short duration passages through the plane of the host galaxy does the FUV radiation flux become small enough to allow the ISM to recombine and potentially form stars. An important requirement of the model is that many dSph galaxies should possess extended and very massive dark matter halos (with virial temperature  $\gtrsim 10^4$  K), allowing them to keep the warm photoionized ISM with temperature  $T \sim 10^4$  K gravitationally bound. There is a growing number of evidence supporting the idea of the dSph galaxies being more massive than the predictions of the mass-follows-light King model (Odenkirchen et al. 2001; Kleyna et al. 2001; Hayashi et al. 2003).

The Sculptor dSph is located relatively close to the Milky Way ( $< 80$  kpc), and is close to the southern Galactic pole. According to the photoevaporation model of MCB, it is expected that the ionizing radiation escaping from the Galactic disk should affect significantly the Sculptor HI clouds. Because the Sun is located much closer to the Galactic center than to the Sculptor dSph, the photoionized regions of the clouds would be seen approximately face-on. In the photoevaporation scenario, the photoionized gas expands with a speed comparable to its sound speed ( $\sim 10$  km s $^{-1}$ ). First it moves normally to the HI cloud surface. If the H II gas stays gravitationally bound to the galaxy, it will soon decline from the normal direction. As a result, the H $_{\alpha}$  spectral line from the photoionized gas is expected to be blue-shifted by  $\sim 5 - 10$  km s $^{-1}$  relatively to the 21 cm spectral line from the neutral cloud.

Weiner et al. (2001) detected H $_{\alpha}$  emission from the SW cloud with a flux of  $220 \pm 23$  mR. The heliocentric radial velocity of the ionized gas is  $V_{HII} = 97 \pm 3 \pm 5$  km s $^{-1}$  (formal / systematic errors) (B. J. Weiner 2001, private communication). Figure 7 shows both the H $_{\alpha}$  detection and the HI spectral line integrated over the same area. The HI line has a peak at  $V_{HI} \simeq 109$  km s $^{-1}$  (which is virtually identical to the stellar radial velocity). The H II gas appears to be blue-shifted by  $V_{HI} - V_{HII} = 12 \pm 8$  km s $^{-1}$  relative to the HI cloud, which is consistent with the prediction of the photoevaporation model of MCB. More accurate measurements of the radial velocity of the H $_{\alpha}$  emitting gas are required to confirm this result with higher confidence.

Table 3: List of all HVCs within  $10^\circ$  of the Sculptor dSph line of sight (Putman et al. 2002) and within the  $80 \text{ km s}^{-1}$  to  $210 \text{ km s}^{-1}$  velocity range.

Catalog designation	RA (J2000)	DEC (J2000)	$\Delta\alpha$	$V_{LSR}$ (km s $^{-1}$ )	$\Delta V$ (km s $^{-1}$ )
HVC 1520	$0^h 50.3^m$	$-34^\circ 4.0'$	$2.08^\circ$	140	39
HVC 1427	$0^h 56.1^m$	$-35^\circ 53.0'$	$2.33^\circ$	126	25
HVC 1550	$0^h 48.8^m$	$-32^\circ 59.0'$	$2.48^\circ$	113	12
HVC 1634	$0^h 46.8^m$	$-31^\circ 20.0'$	$3.68^\circ$	138	37
HVC 1640	$0^h 42.4^m$	$-34^\circ 40.0'$	$3.79^\circ$	160	59
HVC 1547	$0^h 47.2^m$	$-37^\circ 11.0'$	$4.36^\circ$	141	40
HVC 1625	$0^h 42.0^m$	$-36^\circ 4.0'$	$4.41^\circ$	160	59
HVC 1540	$0^h 47.3^m$	$-38^\circ 20.0'$	$5.30^\circ$	164	63
HVC 1462	$0^h 55.7^m$	$-39^\circ 22.0'$	$5.73^\circ$	144	43
HVC 1723	$0^h 31.7^m$	$-36^\circ 29.0'$	$6.45^\circ$	202	101
HVC 912	$1^h 31.3^m$	$-34^\circ 53.0'$	$6.54^\circ$	107	6
HVC 1791	$0^h 26.6^m$	$-35^\circ 52.0'$	$7.22^\circ$	146	45
:HVC 1569	$0^h 43.1^m$	$-40^\circ 8.0'$	$7.27^\circ$	186	85
:HVC 1616	$0^h 38.6^m$	$-39^\circ 45.0'$	$7.42^\circ$	158	57
HVC 1908	$0^h 23.0^m$	$-32^\circ 49.0'$	$7.82^\circ$	129	28
HVC 1825	$0^h 22.0^m$	$-35^\circ 40.0'$	$8.08^\circ$	171	70
HVC 1901	$0^h 20.5^m$	$-33^\circ 37.0'$	$8.25^\circ$	198	97
HVC 3	$0^h 21.9^m$	$-30^\circ 58.0'$	$8.53^\circ$	109	8
HVC 732	$1^h 42.4^m$	$-32^\circ 22.0'$	$8.95^\circ$	111	10
HVC 1932	$0^h 15.7^m$	$-33^\circ 7.0'$	$9.29^\circ$	146	45
HVC 1280	$1^h 20.4^m$	$-42^\circ 7.0'$	$9.30^\circ$	148	47
:HVC 1614	$0^h 36.6^m$	$-42^\circ 4.0'$	$9.56^\circ$	145	44
HVC 1922	$0^h 13.6^m$	$-33^\circ 53.0'$	$9.67^\circ$	162	61
:HVC 1651	$0^h 30.6^m$	$-41^\circ 38.0'$	$9.84^\circ$	171	70
CHVC 1104	$1^h 35.5^m$	$-40^\circ 38.0'$	$9.86^\circ$	120	19
HVC 1031	$1^h 41.0^m$	$-39^\circ 23.0'$	$9.96^\circ$	101	0

Table 4: List of all HVCs within  $10^\circ$  of the Sculptor dSph line of sight (Putman et al. 2002) and outside of the  $80 \text{ km s}^{-1}$  to  $210 \text{ km s}^{-1}$  velocity range.

Catalog designation	RA (J2000)	DEC (J2000)	$\Delta\alpha$	$V_{LSR}$ (km s $^{-1}$ )	$\Delta V$ (km s $^{-1}$ )
HVC 1247	$1^h 44^m$	$-33^\circ 52.0'$	$0.90^\circ$	-212	312
HVC 1292	$1^h 0.7^m$	$-32^\circ 47.0'$	$0.93^\circ$	-180	280
CHVC 1387	$0^h 58.0^m$	$-35^\circ 1.0'$	$1.38^\circ$	-243	343
HVC 1175	$1^h 5.4^m$	$-32^\circ 52.0'$	$1.38^\circ$	-140	240
HVC 1461	$0^h 53.8^m$	$-34^\circ 31.0'$	$1.54^\circ$	-167	267
HVC 1192	$1^h 0.3^m$	$-31^\circ 2.0'$	$2.68^\circ$	-182	282
HVC 1385	$0^h 54.9^m$	$-31^\circ 15.0'$	$2.70^\circ$	-191	291
HVC 1538	$0^h 49.8^m$	$-31^\circ 54.0'$	$2.83^\circ$	-170	270
:HVC 1411	$0^h 57.9^m$	$-36^\circ 57.0'$	$3.27^\circ$	-205	305
HVC 1624	$0^h 44.4^m$	$-33^\circ 56.0'$	$3.28^\circ$	-199	299
HVC 1644	$0^h 45.5^m$	$-32^\circ 8.0'$	$3.46^\circ$	-137	237
HVC 1567	$0^h 49.3^m$	$-30^\circ 50.0'$	$3.68^\circ$	-191	291
HVC 1251	$0^h 56.8^m$	$-30^\circ 4.0'$	$3.71^\circ$	-143	243
HVC 1719	$0^h 42.4^m$	$-31^\circ 43.0'$	$4.23^\circ$	-152	252
HVC 1021	$1^h 21.4^m$	$-34^\circ 54.0'$	$4.55^\circ$	-88	188
HVC 1706	$0^h 37.4^m$	$-34^\circ 45.0'$	$4.82^\circ$	-166	266
HVC 1532	$0^h 51.0^m$	$-28^\circ 42.0'$	$5.38^\circ$	-202	302
HVC 854	$1^h 28.6^m$	$-33^\circ 23.0'$	$5.93^\circ$	-121	221
HVC 892	$0^h 54.2^m$	$-27^\circ 43.0'$	$6.13^\circ$	-212	312
HVC 707	$1^h 23.6^m$	$-30^\circ 0.0'$	$6.21^\circ$	-164	264
HVC 1818	$0^h 30.0^m$	$-33^\circ 43.0'$	$6.27^\circ$	-172	272
HVC 615	$0^h 59.6^m$	$-27^\circ 22.0'$	$6.34^\circ$	-256	356
CHVC 1664	$0^h 35.7^m$	$-37^\circ 52.0'$	$6.47^\circ$	215	114
HVC 1903	$0^h 31.0^m$	$-31^\circ 31.0'$	$6.52^\circ$	-192	292
:HVC 879	$1^h 32.2^m$	$-34^\circ 23.0'$	$6.67^\circ$	-155	255
HVC 941	$1^h 32.3^m$	$-35^\circ 34.0'$	$6.87^\circ$	-83	183
HVC 1499	$0^h 51.2^m$	$-40^\circ 31.0'$	$7.04^\circ$	-110	210
CHVC 630	$1^h 20.7^m$	$-28^\circ 12.0'$	$7.05^\circ$	-197	297
HVC 764	$1^h 33.4^m$	$-32^\circ 22.0'$	$7.09^\circ$	-96	196
HVC 698	$1^h 30.0^m$	$-30^\circ 11.0'$	$7.24^\circ$	-93	193
HVC 588	$1^h 1.9^m$	$-26^\circ 28.0'$	$7.25^\circ$	-268	368
HVC 673	$1^h 28.4^m$	$-29^\circ 28.0'$	$7.36^\circ$	-118	218
HVC 1777	$0^h 26.4^m$	$-36^\circ 27.0'$	$7.43^\circ$	255	154
CHVC 542	$0^h 54.1^m$	$-25^\circ 59.0'$	$7.84^\circ$	-240	340
HVC 1753	$0^h 25.9^m$	$-37^\circ 31.0'$	$7.93^\circ$	-130	230
HVC 219	$0^h 36.2^m$	$-27^\circ 40.0'$	$7.94^\circ$	-168	268
HVC 827	$1^h 41.8^m$	$-34^\circ 32.0'$	$8.65^\circ$	-97	197
HVC 1592	$0^h 39.2^m$	$-41^\circ 37.0'$	$8.92^\circ$	-100	200
HVC 1794	$0^h 20.1^m$	$-37^\circ 38.0'$	$9.03^\circ$	-131	231
CHVC 1079	$1^h 35.5^m$	$-39^\circ 36.0'$	$9.21^\circ$	-112	212
HVC 432	$0^h 38.2^m$	$-25^\circ 42.0'$	$9.32^\circ$	-140	240
HVC 1852	$0^h 15.6^m$	$-36^\circ 5.0'$	$9.43^\circ$	-124	224
HVC 1556	$0^h 42.6^m$	$-42^\circ 36.0'$	$9.53^\circ$	-98	198
HVC 1483	$0^h 53.6^m$	$-43^\circ 22.0'$	$9.74^\circ$	226	125
HVC 1641	$0^h 32.0^m$	$-41^\circ 56.0'$	$9.92^\circ$	-94	194

Table 5: Data on the Sculptor HI clouds. The HI masses assume that the clouds are at the distance of the Sculptor dSph.

	Parkes		ATCA	
	Velocity (km s <sup>-1</sup> )	HI mass ( $\times 10^4 M_{\odot}$ [D/79 kpc] <sup>2</sup> )	Velocity (km s <sup>-1</sup> )	HI mass ( $\times 10^4 M_{\odot}$ [D/79 kpc] <sup>2</sup> )
North East	100.2±0.9	4.07±0.18	99.7±1.7	2.84±0.23
South West	105.1±0.3	19.33±0.24	110.2±1.6	8.67±0.68
Central 15' × 15'	106.3±0.7	0.61±0.02	...	(-1.13±0.27) <sup>a</sup>
Total	104.1±0.4	23.35±0.32	109.3±2.0	8.68±0.83

---

<sup>a</sup>See text for details

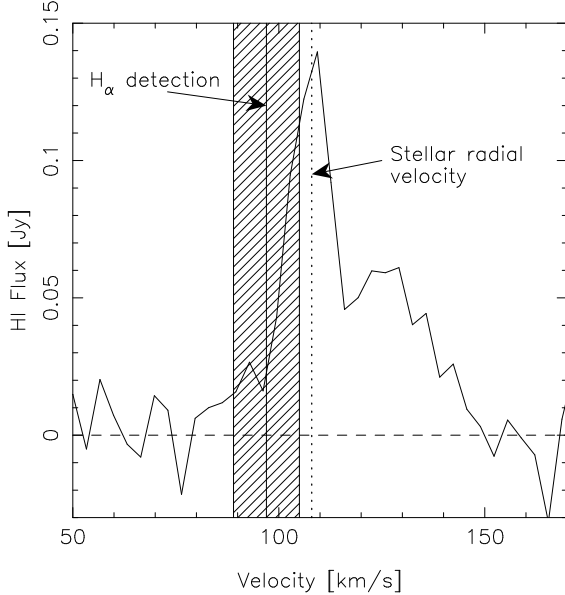


Fig. 7.—  $H_{\alpha}$  detection from the Sculptor dSph (Weiner et al. 2001; B. J. Weiner 2001, private communication). Vertical filled stripe corresponds to the radial velocity of the  $H_{\alpha}$  emission from the southwest HI cloud inside a circle with a radius  $5'$  centered at  $\alpha_{2000} = 0^{\text{h}}58^{\text{m}}22^{\text{s}}$ ,  $\delta_{2000} = -34^{\circ}00'$ . The width of the stripe reflects both formal and systematic errors. We also show the HI spectral line from the ATCA data integrated within the same circle area (solid line) and the stellar radial velocity of the Sculptor dSph (vertical dotted line).

Another interesting feature of Figure 7 is the presence of a red-shifted tail in the HI spectral line. Both analytical (Bertoldi & McKee 1990) and numerical (Lefloch & Lazareff 1994) calculations showed that under a wide range of initial conditions photoevaporating interstellar clouds tend to a quasi-equilibrium cometary state. The cometary tail in these models consists of the neutral gas accelerated away from the cloud. The gas in the tail is neutral because it is shielded from the ionizing radiation by the bulk of the cloud. The red-shifted HI gas in Figure 7 could be a cometary tail of the photoevaporating cloud.

#### 4. Conclusions

New observations of the HI gas in a large area of  $7^{\circ} \times 7^{\circ}$  around the Sculptor dSph are presented. Combination of single-dish (Parkes) and interferometric (ATCA) observations allowed us to achieve both large angular coverage and high angular resolution. These new data sets are of significantly higher resolutions than any other previously released data sets in the line of sight of the Sculptor dSph. Our principal results are:

1. Large angular coverage is required in order to claim to understand the HI properties of dSph

galaxies. Our new data now shows the full extent of the C98 clouds. The size of these clouds is found to be much larger than the largest angular scale ( $\sim 22'$ ) the C98 observations were sensitive to.

2. The single-dish Parkes radiotelescope observations give a total HI mass for the C98 clouds of  $2.3 \times 10^5 [D/79\text{kpc}]^2 M_\odot$ . The heliocentric radial velocity of the gas is  $104 \text{ km s}^{-1}$ .
3. Arguments that the C98 Sculptor clouds are physically associated with the dwarf, thus at a distance of 79 kpc, are presented, the most important ones being the closeness of the radial velocities for the HI gas and the stars ( $\Delta V = 4 \pm 3 \text{ km s}^{-1}$  based on the Parkes data), and the location of almost all of the HI emission (88% of the total flux) within the stellar body of the dwarf (in projection). The unlikely possibility of the clouds being part of a general ensemble of compact HVCs cannot be ruled out on the basis of the available data.
4. The combination of the present HI observations with the  $\text{H}_\alpha$  emission line detection from the southwest cloud (Weiner et al. 2001) gives support to the FUV radiation harassment model of MCB. The difference in radial velocities between the neutral and ionized gas is found to be  $12 \pm 8 \text{ km s}^{-1}$ , which is consistent with the Sculptor clouds being photoevaporated by the Milky Way LyC radiation.

We are grateful to Lister Staveley-Smith for helpfull discussions. We acknowledge financial suport from NSERC, Canada and FQRNT, Québec. The Australia Telescope Compact Array and Parkes telescope are part of the Australia Telescope which is funded by the Commonwealth of Australia for operation as a National Facility managed by CSIRO.

## REFERENCES

Andersen, R.-P. & Burkert, A. 2000, *ApJ*, 531, 296

Barnes, D. G. et al. 2001, *MNRAS*, 322, 486

Bertoldi, F. & McKee, C. F. 1990, *ApJ*, 354, 529

Blais-Ouellette, S., Amram, P., & Carignan, C. 2001, *AJ*, 121, 1952

Blitz, L. & Robishaw, T. 2000, *ApJ*, 541, 675

Burkert, A. & Ruiz-Lapuente, P. 1997, *ApJ*, 480, 297

Carignan, C. 1998, *Highlights in Astronomy*, 11, 121

Carignan, C., Beaulieu, S., Côté, S., Demers, S., & Mateo, M. 1998, *AJ*, 116, 1690 (C98)

de Blok, W. J. G., McGaugh, S. S., Bosma, A., & Rubin, V. C. 2001, *ApJ*, 552, L23

de Vaucouleurs, G., de Vaucouleurs, A., Corwin, H. G., Jr., Buta, R. J., Paturel, G., & Fouque, P. 1991, *Third Reference Catalogue of Bright Galaxies* (New York: Springer-Verlag)

Ferrara, A. & Tolstoy, E. 2000, *MNRAS*, 313, 291

Grebel, E. K. 1997, *Reviews of Modern Astronomy*, 10, 29

Grebel, E. K. 1998, *Highlights in Astronomy*, 11, 125

Hayashi, E., Navarro, J. F., Taylor, J. E., Stadel, J., & Quinn, T. 2003, *ApJ*, 584, 541

Irwin, M. & Hatzidimitriou, D. 1995, *MNRAS*, 277, 1354

Jerjen, H., Freeman, K. C., & Binggeli, B. 1998, *AJ*, 116, 2873

Kleyna, J. T., Wilkinson, M. I., Evans, N. W., & Gilmore, G. 2001, *ApJ*, 563, L115

Lefloch, B. & Lazareff, B. 1994, *A&A*, 289, 559

Mac Low, M. & Ferrara, A. 1999, *ApJ*, 513, 142

Mashchenko, S., Carignan, C., & Bouchard, A. 2003, *ApJ*, submitted (astro-ph/0203317) (MCB)

Mateo, M. L. 1998, *ARA&A*, 36, 435

Mathewson, D. S. & Ford, V. L. 1984, in *IAU Symp. 108: Structure and Evolution of the Magellanic Clouds*, 125

Moore, B., Ghigna, S., Governato, F., Lake, G., Quinn, T., Stadel, J., & Tozzi, P. 1999, *ApJ*, 524, L19

Odenkirchen, M. et al. 2001, AJ, 122, 2538

Oosterloo, T., Da Costa, G. S., & Staveley-Smith, L. 1996, AJ, 112, 1969

Putman, M. E. et al. 2002, AJ, 123, 873

Schweitzer, A. E., Cudworth, K. M., Majewski, S. R., & Suntzeff, N. B. 1995, AJ, 110, 2747

Spaans, M. & Norman, C. A. 1997, ApJ, 483, 87

van Zee, L. 2001, AJ, 121, 2003

Weiner, B. J., Vogel, S. N., & Williams, T. B. 2001, preprint (astro-ph/0109055)

Young, L. M. & Lo, K. Y. 1996, ApJ, 462, 203

— 1997, ApJ, 490, 710